Asian Journal of Chemistry; Vol. 38, No. 4 (2026), 1007-1012
ASIAN JOURNAL OF CHEMISTRY
https://doi.org/10.14233/ajchem.2026.35488

Eco-Friendly Fabrication and Chemical Profiling of Termite Wing-Derived Novel Chitosan-Silver Nanoparticles with Antibacterial and Antibiofilm Potentials

KARUNAKARAN SARAVANAN[1], RAJA MANICKAM[2], KARTHIK SHANMUGAM[3], PALANISAMY ARULSELVAN[4,*] and SHANMUGAMPREMA DEEPANKUMAR[5]

[1]Department of Chemical Engineering, KPR Institute of Engineering and Technology, Avinashi Road, Arasur, Coimbatore-641407, India
[2]Department of Chemistry, Sona College of Technology, Salem-636005, India
[3]Department of Biochemistry, RVS Siddha Medical College and Hospital, Coimbatore-641402, India
[4]Department of Biochemistry, Karpagam Academy of Higher Education (Deemed to be University), Coimbatore-641021, India
[5]Department of Research Analytics, Saveetha Dental College and Hospitals, Saveetha Institute of Medical and Technical Sciences, Saveetha University, Chennai-602105, India

*Corresponding author: E-mail: arulbio@gmail.com

Received: 19 December 2025 *Accepted*: 19 February 2026 *Published online*: 8 April 2026 AJC-22322

This study reports a sustainable route for preparing chitosan-capped silver nanoparticles (CSAg NPs) using chitosan obtained from termite wings (*Odontotermes obesus*) through a straightforward one-pot synthesis. The method enabled the reduction of Ag^+ ions to metallic silver under mild conditions, producing stable nanoparticles without using harsh reagents. UV-visible spectroscopy verified that nanoparticles were formed as a result of the reaction of chitosan with silver nitrate, which exhibited a surface plasmon resonance (SPR) peak at 425 nm. The X-ray diffraction data suggested that the resulting material was crystalline in nature; however, Fourier transform infrared (FTIR) spectra demonstrated that the hydroxyl and amino functionalities on the chitosan molecules were present and thus may have played a role in the stabilisation of the nanoparticles produced. Further analysis of morphology and element composition was carried out by scanning electron microscopy (SEM) and energy dispersive X-ray (EDX) spectroscopy to further verify the particle structure and presence of silver in the samples. The synthesised CSAg NPs exhibited excellent antibacterial activity at a concentration of 200 µg/mL, with inhibition zones of 15.3 ± 1.52 mm against *Streptococcus mutans* and 16.6 ± 1.52 mm against *Streptococcus sobrinus*. In addition, the nanoparticles demonstrated strong antibiofilm action against both oral infections. The prepared CSAg NPs showed pronounced antibiofilm activity against oral pathogens, indicating their potential application in controlling dental infections. The use of termite-wing-derived chitosan as a precursor for nanoparticle fabrication is reported here for the first time, offering a novel, environmentally friendly strategy for developing antimicrobial materials targeting biofilm-associated oral diseases.

Keywords: Termites wings, Chitosan, Silver nanoparticles, *Streptococcus mutans*, *Streptococcus sobrinus*, Biofilm.

INTRODUCTION

The oral cavity is a dynamic and complex ecosystem in which a diverse spectrum of microorganisms dwells, either as harmless commensals or as opportunistic pathogens in the host environment [1]. Many of these microorganisms represent little hazard on their own, but their capacity to form organised biofilms is crucial in the development of oral diseases. The biofilm produced by bacteria contains an extracellular polymeric (exopolysaccharide) matrix that shields the bacteria from antimicrobial agents and host immune system responses which increases their ability to survive and persist. Biofilm formation on the surface of teeth is a critical factor in the development of dental caries because it facilitates solid bacterial attachment and creates localised environments around each tooth that contribute to the acid-mediated decalcification of enamel and dentin. When these biofilms form on the teeth of individuals who consume high amounts of fermentable carbohydrates and do not maintain good oral hygiene, they can be very cariogenic and produce acid that slowly breaks down both the enamel and the dentin of tooth causing eventual tooth loss [2]. Although there has been significant improvement in the effectiveness of antimicrobial therapies, the effective removal of bacteria associated with biofilms continues to be a problem. In response

to this difficulty, interest in other methods or applications in addition to traditional antimicrobial therapies has increased. One such application is the use of nanopharmaceuticals in oral health care [3-7].

Both chitosan, a non-toxic and biocompatible polymer derived from the deacetylation of chitin and silver nanoparticles (Ag NPs), which are well known for their broad-spectrum antimicrobial and antioxidant activities, have shown significant antibacterial activity against oral pathogens. Ag NPs are capable of inhibiting various types of microorganisms and have also been shown to be active against multiple viral pathogens including hepatitis B virus, herpes simplex virus-1 and HIV. Ag NPs exhibit a bactericidal effect primarily through the interaction and disruption of bacterial cell membranes and walls resulting in damage to the structure and death of the bacterial cells [8-14].

Green or biosynthetic routes to Ag NPs production, utilizing plant extracts, minerals, or biological macromolecules as reducing and stabilizing agents, have gained traction over the past decade due to their cost-effectiveness, environmental friendliness and potential to enhance antimicrobial performance. Combinations of AgNPs with chitosan have shown promising clinical outcomes, including improved caries arrest and low toxicity profiles in some trials [15-19]. Prior studies have successfully produced chitosan-based AgNPs from discarded crustacean material and demonstrated strong antibacterial activity against clinical isolates [20,21]. Notably, the extraction of chitosan from termite wings has not been explored. In this study, we therefore isolate chitosan from the termite wings to synthesise chitosan-stabilised silver nanoparticles (CSAg NPs), evaluate the reducing capacity of the termite-derived chitosan and assess the resulting nanoparticles for antibacterial and antibiofilm activity against cariogenic bacteria associated with dental caries.

EXPERIMENTAL

Collection of termite wings: About 50 g of termite wings were gathered during the rainy season in Mayiladuthurai, India. The insects were identified as *Odontotermes obesus*. The wings were carefully rinsed with distilled water to remove dust and surface contaminants, then placed in a desiccator and allowed to air-dry at room temperature until all moisture was eliminated. Then, the dried samples were stored in air-tight containers until further processing.

Extraction of chitosan from termite wings: The chitin product was recovered by milling dried termite wing samples into a fine powder. Chitin was then demineralised and decolourised in order to purify the powdered chitin and remove all contaminants. Following the purification of powdered chitin, it was treated with 50% NaOH for deacetylation in order to break away the acetyl group and produce chitosan (CS) that had been formed during the deacetylation process. Finally, the mixture was thoroughly rinsed with MilliQ water until a neutral pH was achieved, then the end product was dried and kept in a desiccator for further usage.

Synthesis of chitosan-stabilised silver nanoparticles (CS-Ag NPs): Chitosan-stabilised silver nanoparticles (CSAg NPs) were synthesised using 0.5g of CS, which was dissolved in a 2% acetic acid solution to obtain a 2.0% (w/v) chitosan solution. Then, 0.1 g of silver precursor was added and the mixture was stirred for 45 min to promote nanoparticle formation. The resulting CSAg NP precipitate was isolated by repeated washing and centrifugation, then dried and stored for characterisation.

Characterisation: Formation of CSAg NPs was confirmed by UV-spectrophotometer (Shimadzu, Japan). Further surface area and morphology of the CSAg NPs were analysed using a scanning electron microscope (SEM) (JSM-IT 200, Japan). Fourier transform infrared spectroscopy (FT-IR) (Perkin-Elmer spectrum RX-1, USA) examined stretching frequencies and spectrum within the range of 4000-400 cm^{-1} and X-ray diffraction (XRD) patterns were recorded using a Model D/max-RC X-ray diffractometer. Dynamic light scattering (DLS) analysis was performed using a Malvern Zetasizer Nano series instrument to determine the particle size distribution of the synthesised CS-Ag NPs.

Antibacterial activity: The dental pathogens of *Streptococcus mutans* and *Streptococcus sobrinus* were procured from Saveetha Dental College and Hospitals, Chennai, India. The antibacterial test was carryout using the agar diffusion method on Brain Heart Infusion (BHI) agar. McFarland 0.5 suspensions of bacterial strains were spread onto agar plates and CSAg NPs based discs were placed on the inoculated plates. After 48 h of incubation at 37 ºC, the zones of inhibition were measured using a digital caliper.

Biofilm assessment: Six CSAg NPs discs with dimensions of 7 mm in diameter and 1 mm in thickness were placed in tubes each containing 1 mL of a bacterial suspension with a concentration of 10^8 CFU/mL. After a period of 3 days, the discs were removed and submerged in sterile PBS (phosphate buffered saline) and subsequently transferred to tubes containing 1 mL of Brain Heart Infusion (BHI) broth. Detached biofilms were vortexed, diluted in series, plated on BHI agar and incubated for 24 to 48 h. The total colony-forming units per milliliter on each disk were determined using colony counts and dilution factor.

Statistical analysis: All analytical measurements were carried out in triplicate and experimental values are reported as mean ± standard deviation (SD). Statistical evaluation of the formulations was performed using SPSS software (version 16) which was employed to organize the data and assess variation.

RESULTS AND DISCUSSION

UV-Vis analysis: Fig. 1 shows the UV absorption spectrum of synthesise CSAg NPs. The colour of the chitosan solution changed from colourless to light yellow to yellowish brown during the synthesis of CSAg NPs, signifying the reduction of Ag^+. The colourless chitosan solution turned light yellow to yellowish-brown when the characteristic peak of CSAg NPs was observed at 425 nm, indicating the decrease of Ag^+. According to previous studies, the characteristic absorption peak of CSAg NPs typically appears in the 400-500 nm range [22-24].

Surface morphology and EDX analysis: The SEM images (Fig. 2) reveal that the CSAg NPs exhibit an irregular

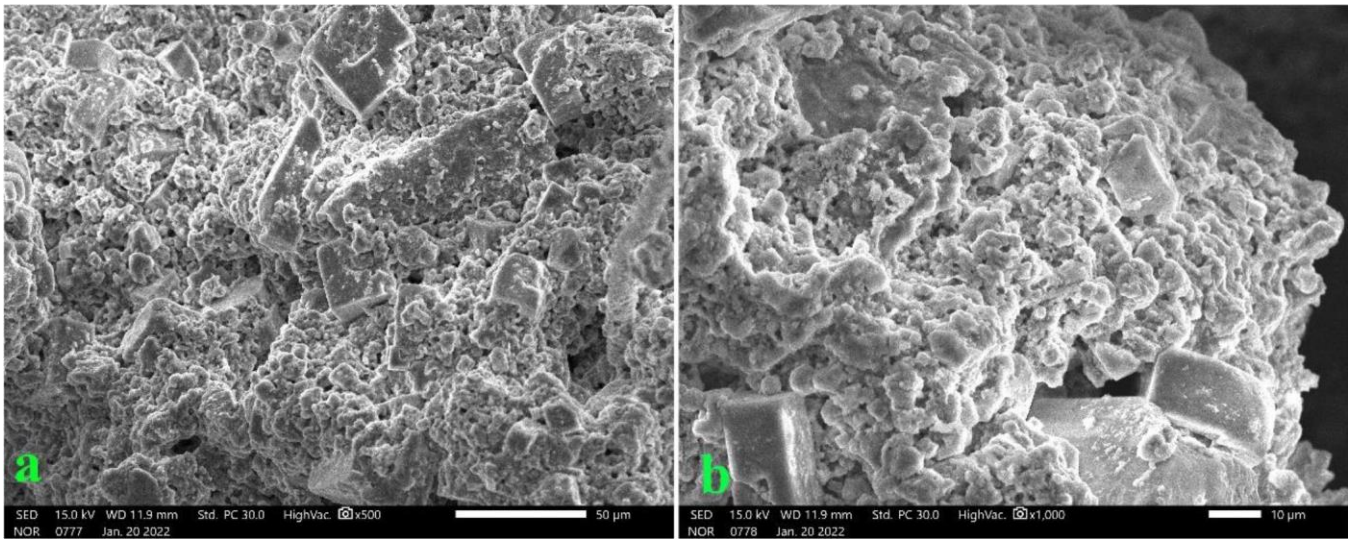

Fig. 2. SEM images of chitosan-based silver nanoparticles (CSAg NPs) at 500× (a) and 1000× magnification (b)

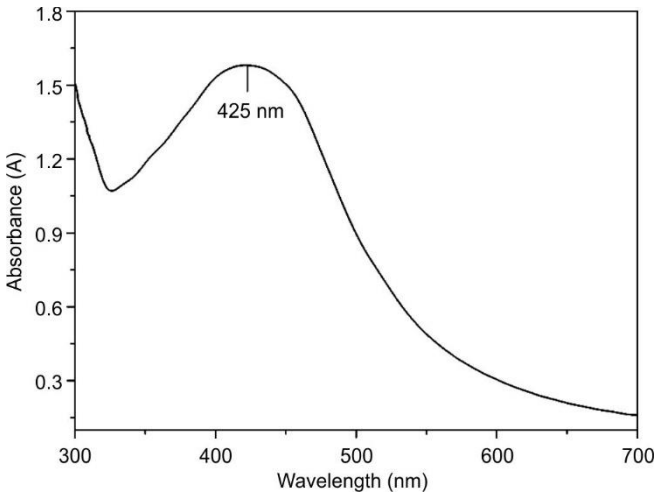

Fig. 1. UV spectrum of chitosan-based silver nanoparticles (CSAg NP)

and rough surface morphology with clear aggregation of particles. At higher magnification, the nanoparticles appear clustered and embedded within the chitosan matrix, indicating effective capping and stabilization. The porous and heterogeneous surface structure suggests a high surface area, which may contribute to enhanced antimicrobial and antibiofilm activity. The EDX spectrum (Fig. 3) confirms the elemental composition of the synthesised CSAg NPs, showing dominant peaks corresponding to silver (Ag) along with minor calcium (Ca) signals. The high intensity of Ag peaks with a mass percentage of about 95.05% verifies the successful formation and predominance of Ag NPs in the sample. The presence of Ca (4.95%) can be attributed to residual mineral content naturally associated with the termite wing-derived chitosan, originating from the insect exoskeleton. These results confirm that Ag NPs were effectively formed and stabilized within the chitosan matrix, with trace calcium originating from the biological precursor.

FTIR spectral studies: FTIR analysis was carried out to identify the functional groups and bond linkages involved in reducing silver ions and stabilizing the resulting CSAg NPs.

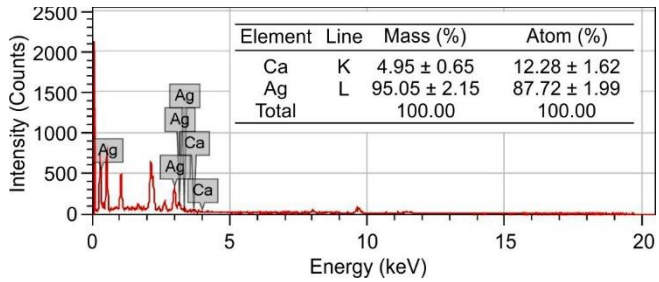

Fig. 3. EDX spectrum of CSAg NPs

Several characteristic absorption bands at 3435.52, 2924.97, 2854.78, 2426.58, 1643.50, 1571.69, 1384.24, 1154.87, 1114.29, 1071.41, 1020.23, 833.41 and 651.41 cm^{-1} are observed in Fig. 4 The broad peak near 3435.52 cm^{-1} corresponds to O–H stretching, indicating the presence of alcohol or phenolic groups while the bands at 2924.97 and 2854.78 cm^{-1} arise from C–H stretching vibrations typical of alkyl chains. A weaker band around 2426.58 cm^{-1} may reflect the presence of C≡C or C≡N stretching. The peak at 1643.50 cm^{-1} corresponds to C=O stretching, suggesting carbonyl-containing groups such as aldehydes, ketones or carboxylic acids. The band at 1571.69 cm^{-1} corresponds to C=C stretching, while the absorption at 1384.24 cm^{-1} reflects C–H bending of alkyl groups. The absorption peaks at 1154.87 and 1071.41 cm^{-1} correspond to C–O stretching vibrations, whereas the band at 1114.29 cm^{-1} is assigned to C–N stretching, confirming the existence of amine groups. The vibrations at 1020.23 cm^{-1} are due to alkyl C–H bending, while the peaks at 833.41 and 651.41 cm^{-1} are caused by out-of-plane aromatic C–H bending. Amino and hydroxyl groups in termite wing-derived chitosan facilitate the reduction of Ag^{+} ions and stabilize the formed Ag NPs through surface coordination. These functional groups also enhance the antibacterial activity of the synthesised CSAg NPs.

XRD studies: Powder XRD analysis was performed to determine the crystalline structure of the biosynthesised CSAg NPs and the diffraction pattern was recorded over a 2θ range of 10-80º, as shown in Fig. 5a. Well-defined diffraction

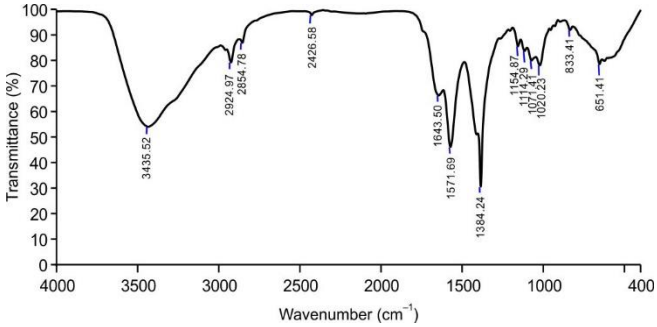

Fig. 4. FTIR spectrum of CSAg NPs

peaks occurring at approximately 38.26º, 44.47º, 64.71º, 77.74º, 81.90º and 98.37º correspond to (1 1 1), (2 0 0), (2 2 0), (3 1 1), (2 2 2) and (4 0 0) reflections, respectively, confirm the face-centered cubic (FCC) structure of CSAg NPs, in accordance with ICSD file no. 96-901-2432. Furthermore, the X-ray diffraction pattern of chitosan (CS) revealed a distinct peak at 2θ = 21.68º. In comparison, the diffraction pattern of CSAg NPs showed clear peaks for silver and calcium. This indicates that the chitosan-silver nanoparticles were successfully formed. The characteristic peaks in the CSAg NPs pattern confirm the presence of crystalline silver within the chitosan matrix. Similar diffraction peaks have also been reported in earlier studies [25].

The sharp peak suggested the presence of bioorganic/proteins in the nanoparticles synthesis process [26]. The XRD pattern clearly demonstrated the reduction of silver ions to AgO by stabilizing chitosan at the specified reaction conditions. The analysis of the pattern demonstrated the presence of reflection planes, confirming the existence of a face-centered cubic structure of metallic silver. No peaks were identified, suggesting the absence of any impurity crystalline phases [27,28]. Furthermore, the dynamic light scattering (DLS) analysis confirmed the size of the synthesised materials were in nanoform with an average particles distribution was ranged from 10 nm to 130 nm and its peaked was observed around 80 nm (Fig. 5b).

Antibacterial and antibiofilm activity: The antibiofilm and antibacterial activity of CSAg NPs were evaluated against two dental pathogens *viz. S. mutans* and *S. sobrinus*. The data (Table-1) showed an approximately normal distribution allowing the use of standard parametric analysis. Antibacterial activity was evaluated using zone-of-inhibition measurements

TABLE-1
ANTIBACTERIAL ACTIVITY DATA OF SYNTHESISED NANOPARTICLES (CSAg NPs)

Pathogens	Conc. (μg/mL)	Average (mm)	S.D. (±)
S. mutans	50	8.66 ± 0.58	0.58
	100	13.66 ± 1.15	1.15
	200	15.33 ± 1.53	1.53
S. sobrinus	50	12.00 ± 1.00	1.00
	100	15.66 ± 1.15	1.15
	200	16.66 ± 1.52	1.52

and colony counting after 24 h, providing both quantitative antimicrobial effectiveness and an indication of early biofilm persistence.

At the highest concentration tested (200 μg mL^{-1}), CSAg NPs produced clear, reproducible antibacterial effects, with mean inhibition zones of 15.33 ± 1.52 mm for *S. mutans* and 16.66 ± 1.52 mm for *S. sobrinus* (Table-1). Fig. 6 demonstrated a clear concentration-dependent reduction in viable bacterial counts. The plates treated with 200 μg mL^{-1} showed fewer colonies and reduced confluent growth compared with controls, whereas intermediate reductions were observed at 100 μg mL^{-1} and minimal but detectable effects at 50 μg mL^{-1}. This response confirms dose-dependent bactericidal and anti-adhesive activity of CSAg NPs under the tested conditions [29-33]. The enhanced antimicrobial performance is attributed to the small size and large surface area of CSAg NPs, which facilitates strong interaction with bacterial cells and promotes the release of Ag^+ ions. These ions penetrate the bacterial cell wall, disrupt membrane integrity, increase permeability and lead to leakage of intracellular contents, ultimately affecting respiration and nutrient transport [34,35]. Additionally, silver nanoparticles can induce reactive oxygen species (ROS) generation, which further damages DNA and cellular components, accelerating bacterial cell death [36]. The relative contribution of membrane disruption and oxidative stress depends on the nanoparticle size, surface chemistry and concentration [30,37-40].

Termite wing–derived chitosan functions as both a reducing and capping agent during nanoparticle synthesis. The protonated amino groups promote electrostatic interaction with negatively charged bacterial surfaces, enhancing nanoparticle adhesion and localized silver delivery. The hydroxyl and amino groups remaining on the nanoparticle surface stabilize

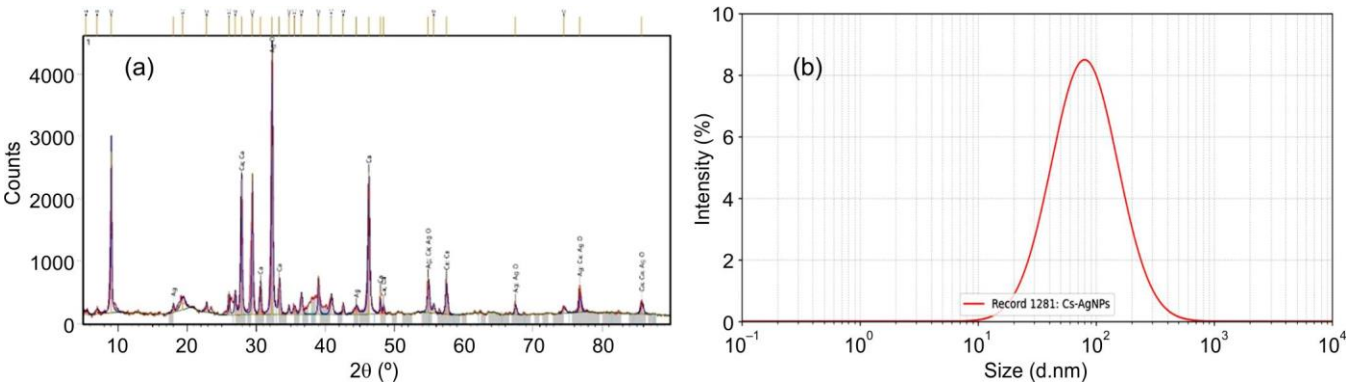

Fig. 5. (a) X-ray diffraction (XRD) pattern and (b) dynamic light scattering (DLS) of CS-Ag NPs

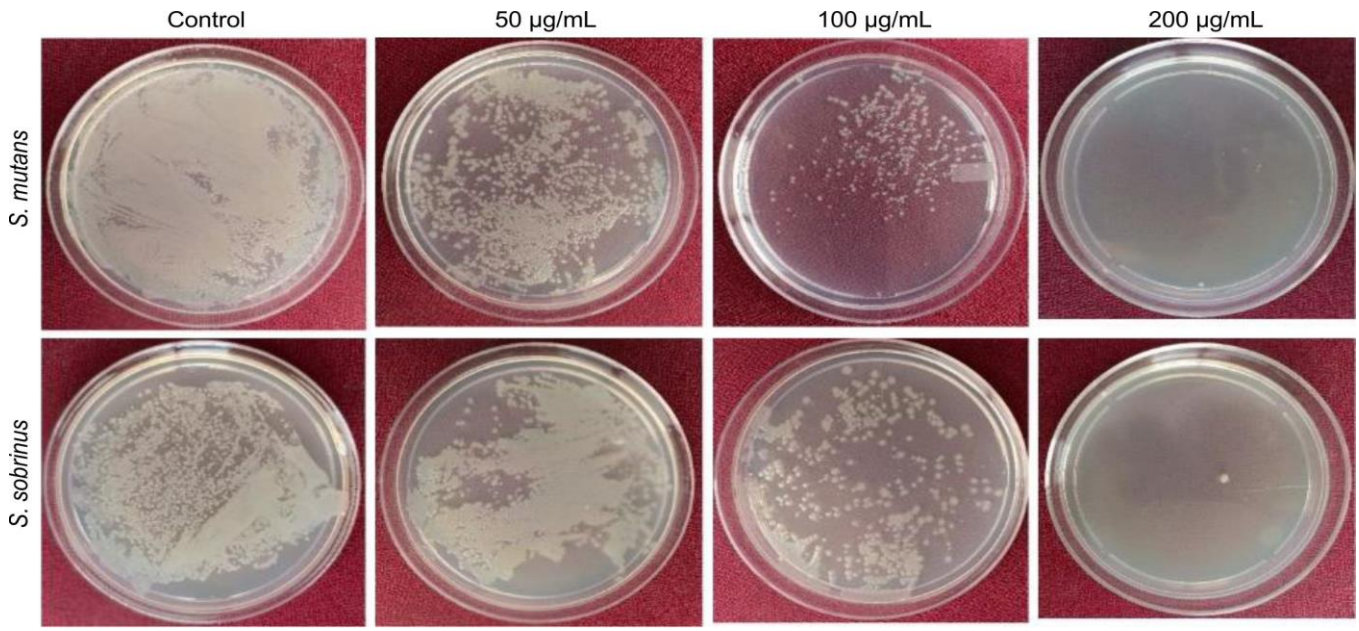

Fig. 6. Biofilm inhibition efficacy of CSAg NPs at different concentrations: control, 50, 100, and 200 µg/mL, showing concentration-dependent reduction in biofilm formation

the colloids and facilitate the close contact with microbial cells, thereby improving antimicrobial efficiency. Chitosan itself also contributes to contact-mediated antibacterial activity by altering membrane permeability and promoting membrane rupture at sufficient local concentration [41,42]. The combined chitosan-silver system therefore provides enhanced bactericidal action compared with either component alone.

The antibiofilm relevance of these findings is particularly important for dental pathogens, which predominantly survive as surface-associated biofilms. CSAg NPs reduced colony-forming units and visibly suppressed early microcolony formation, especially at 200 µg mL^{-1}, suggesting interference with both bacterial adhesion and early biofilm maturation. Although short-term agar assays do not fully represent mature biofilms, the reduction in viable counts and microcolony development indicates inhibition of early biofilm establishment. These observations, together with the sustainable use of termite wing derived chitosan, highlight CSAg NPs as promising antimicrobial and antibiofilm agents for dental applications, warranting further investigation into biocompatibility and long-term performance [43-45].

Statistical results: Post-hoc comparisons between concentrations (Table-2) revealed statistically significant differences between 200 and 50 µg mL^{-1} (mean difference = 6.00 mm, 95% CI: 4.12-7.88, $p < 0.001$) and between 100 and 50 µg mL^{-1} (mean difference = 4.50 mm, 95% CI: 2.62-6.38, $p < 0.001$) indicating strong concentration-dependent antibacterial activity. In contrast, the difference between 200 and 100 µg mL^{-1} was not statistically significant (mean difference = 1.50 mm, 95% CI: -0.38-3.38, $p = 0.114$), suggesting comparable effects at higher concentrations. These results confirm that both 100 and 200 µg mL^{-1} significantly improved antimicrobial performance compared with 50 µg mL^{-1}, while increasing the concentration beyond 100 µg mL^{-1} did not produce a statistically significant additional effect.

Conclusion

This study demonstrates a safe and efficient approach for synthesising silver nanoparticles (Ag NPs) using chitosan derived from *O. obesus*, a termite wing. The biosynthesised CSAg NPs were comprehensively characterized by UV-Visible spectroscopy, FTIR, XRD, SEM and EDAX analyses. FTIR results confirmed the presence of chitosan functional groups, indicating its role in reducing silver ions and stabilizing the nanoparticles through surface capping. The synthesized CSAg NPs exhibited strong antibacterial activity, particularly at higher concentrations, with a significant reduction in the bacterial colony formation, likely due to membrane disruption and oxidative stress–mediated damage. The CSAg NPs showed promising activity against oral pathogens such as *S. mutans* and *S. sobrinus*. These findings highlight the potential of termite-derived CSAg NPs as effective antimicrobial agents for oral health applications. However, further studies are required to elucidate the detailed antibacterial mechanisms

TABLE-2
POST-HOC COMPARATIVE DATA BETWEEN DIFFERENT CONCENTRATIONS

Concentration comparison	Mean difference (mm)	95% CI	*p*-value	Significance
200 *vs*. 50 µg/mL	6.00	[4.12, 7.88]	< 0.001	***
100 *vs*. 50 µg/mL	4.50	[2.62, 6.38]	< 0.001	***
200 *vs*. 100 µg/mL	1.50	[-0.38, 3.38]	0.114	ns

***$p < 0.001$; ns, not significant; CI, confidence interval.

and evaluate cytotoxicity toward mammalian cells to ensure safety and clinical applicability.

CONFLICT OF INTEREST

The authors declare that there is no conflict of interests regarding the publication of this article.

DECLARATION OF AI-ASSISTED TECHNOLOGIES

During the preparation of this manuscript, the authors used an AI-assisted tool(s) to improve the language. The authors reviewed and edited the content and take full responsibility for the published work.

REFERENCES

1. S. Eick, *Monogr. Oral Sci.*, **29**, 1 (2021); https://doi.org/10.1159/000510184.
2. A. Kensche, C. Holder, S. Basche, N. Tahan, C. Hannig and M. Hannig, *Arch. Oral Biol.*, **80**, 18 (2017); https://doi.org/10.1016/j.archoralbio.2017.03.013
3. C.M. Nobre, N. Putz, B. Konig, S. Rupf and M. Hannig, *Front. Bioeng. Biotechnol.*, **8**, 598311 (2020); https://doi.org/10.3389/fbioe.2020.598311
4. C.M.G. Nobre, N. Putz and M. Hannig, *Scanning*, **2020**, 6065739 (2020); https://doi.org/10.1155/2020/6065739
5. C. Hannig, S. Basche, T. Burghardt, A. Al-Ahmad and M. Hannig, *Clin. Oral Investig.*, **17**, 805 (2013); https://doi.org/10.1007/s00784-012-0781-6
6. N.B. Arweiler, *Monogr. Oral Sci.*, **29**, 91 (2021); https://doi.org/10.1159/000510185
7. S. Ahmed, M. Ahmad, B.L. Swami and S. Ikram, *J. Adv. Res.*, **7**, 17 (2016); https://doi.org/10.1016/j.jare.2015.02.007
8. A.A. Yaqoob, H. Ahmad, T. Parveen, A. Ahmad, M. Oves, I.M. Ismail, H.A. Qari, K. Umar and M.N. Mohamad Ibrahim, *Front Chem.*, **8**, 341 (2020a); https://doi.org/10.3389/fchem.2020.00341
9. Y. Sun, *Chem. Soc. Rev.*, **42**, 2497 (2013); https://doi.org/10.1039/C2CS35289C
10. A.M. Grumezescu, E. Andronescu, A.M. Holban, A. Ficai, D. Ficai, G. Voicu, V. Grumezescu, P.C. Balaure and C.M. Chifiriuc, *Int. J. Pharm.*, **454**, 233 (2013); https://doi.org/10.1016/j.ijpharm.2013.06.054
11. L.S. Wang, C.Y. Wang, C.H. Yang, C.L. Hsieh, S.Y. Chen, C.Y. Shen, J.J. Wang and K.S. Huang, *Int. J. Nanomedicine*, **10**, 2685 (2015); https://doi.org/10.2147/IJN.S77410
12. A.A. Yaqoob, K. Umar and M.N.M. Ibrahim, *Appl. Nanosci.*, **10**, 1369 (2020); https://doi.org/10.1007/s13204-020-01318-w
13. P.R. More, S. Pandit, A. De Filippis, G. Franci, I. Mijakovic and M. Galdiero, *Microorganisms*, **11**, 369 (2023); https://doi.org/10.3390/microorganisms11020369
14. L. Lu, R.W.Y. Sun, R. Chen, C.K. Hui, C.M. Ho, J.M. Luk, G.K. Lau and C.M. Che, *Antivir. Ther.*, **13**, 253 (2008); https://doi.org/10.1177/135965350801300210
15. D. Baram-Pinto, S. Shukla, N. Perkas, A. Gedanken and R. Sarid, *Bioconjug. Chem.*, **20**, 1497 (2009); https://doi.org/10.1021/bc900215b
16. J.L. Elechiguerra, J.L. Burt, J.R. Morones, A. Camacho-Bragado, X. Gao, H.H. Lara and M.J. Yacaman, *J. Nanobiotechnol.*, **3**, 6 (2005); https://doi.org/10.1186/1477-3155-3-6
17. Y. Mori, T. Ono, Y. Miyahira, V.Q. Nguyen, T. Matsui and M. Ishihara, *Nanoscale Res. Lett.*, **8**, 93 (2013); https://doi.org/10.1186/1556-276X-8-93
18. K. Khairan, R. Idroes, T.E. Tallei, M.J. Nasim and C. Jacob, *Curr. Nutr. Food Sci.*, **17**, 621 (2021); https://doi.org/10.2174/1573401317999210112201439
19. M. Zargar, A.A. Hamid, F.A. Bakar, M.N. Shamsudin, K. Shameli, F. Jahanshiri and F. Farahani, *Molecules*, **16**, 6667 (2011); https://doi.org/10.3390/molecules16086667
20. R. Kalaivani, M. Maruthupandy, T. Muneeswaran, A. Hameedha Beevi, M. Anand, C.M. Ramakritinan and A.K. Kumaraguru, *Front. Lab. Med.*, **2**, 30 (2018); https://doi.org/10.1016/j.flm.2018.04.002
21. H.V. Tran, L.D. Tran, C.T. Ba, H.D. Vu, T.N. Nguyen, D.G. Pham and P.X. Nguyen, *Colloids Surf. A Physicochem. Eng. Asp.*, **360**, 32 (2010); https://doi.org/10.1016/j.colsurfa.2010.02.007
22. M. Adlim, M.I. Hidayat, N. Azmi and R.F.I. Ramayani, Preparation of Chitosan-Silver Nanoparticles Immobilized onto Pumice for Anti-bacterial Testing Against *Escherichia coli*. In: Proceedings of the 2nd International Conference on Experimental and Computational Mechanics in Engineering, Lecture Notes in Mechanical Engineering, pp. 63-72 (2021); https://doi.org/10.1007/978-981-16-0736-3_7
23. S. Palanisamy, R. David, E. Madav, V. Devi Kannan, V. Rajendran, S. Sampath, M. Z. Ahmed, A. S. Alqahtani, S. Kazmi and P. Asaithambi, *Mater. Technol.*, **39**, 2304428 (2024); https://doi.org/10.1080/10667857.2024.2304428
24. M. Dhanislas, S. Sampath, M. Shamya, J. Joseph, M. Yasasve, M.Z. Ahmed, A.S. Alqahtani, S. Kazmi, P. Asaithambi and A. Suresh, *Mater. Technol.*, **38**, 2269358 (2023); https://doi.org/10.1080/10667857.2023.2269358
25. V. Gopinath, D. MubarakAli, J. Vadivelu, S. Manjunath Kamath, A. Syed and A.M. Elgorban, *Process Biochem.*, **99**, 348 (2020); https://doi.org/10.1016/j.procbio.2020.09.011
26. S. Shankar, A. Rai, B. Ankamwar, A. Singh, A. Ahmad and M. Sastry, *Nat. Mater.*, **3**, 482 (2004); https://doi.org/10.1038/nmat1152
27. K.A. Bogle, S.D. Dhole and V.N. Bhoraskar, *Nanotechnology*, **17**, 3204 (2006); https://doi.org/10.1088/0957-4484/17/13/021
28. R. Zamiri, A. Zakaria, M.S. Husin, Z.A. Wahab and F.K. Nazarpour, *Int. J. Nanomedicine*, **6**, 2221 (2011); https://doi.org/10.2147/IJN.S23830
29. K. Ikuma, A.W. Decho and B.L. Lau, *Front. Microbiol.*, **6**, 591 (2015); https://doi.org/10.3389/fmicb.2015.00591
30. B. Le Ouay and F. Stellacci, *Nano Today*, **10**, 339 (2015); https://doi.org/10.1016/j.nantod.2015.04.002
31. J.L.D.C. Lima, L.R. Alves, J.N.P.D. Paz, M.A. Rabelo, M.A.V. Maciel and M.M.C.D. Morais, *Rev. Bras. Ter. Intensiva*, **29**, 310 (2017); https://doi.org/10.5935/0103-507X.20170039
32. A.T. Khalil, M. Ovais, I. Ullah, M. Ali, Z.K. Shinwari, S. Khamlich and M. Maaza, *Nanomedicine*, **12**, 1767 (2017); https://doi.org/10.2217/nnm-2017-0124
33. S. Karthik, P. Siva, K.S. Balu, R. Suriyaprabha, V. Rajendran and M. Maaza, *Adv. Powder Technol.*, **28**, 3184 (2017); https://doi.org/10.1016/j.apt.2017.09.033
34. M. Ghavam, *BMC Complement. Med. Ther.*, **23**, 299 (2023); https://doi.org/10.1186/s12906-023-04101-w
35. S. Asefian and M. Ghavam, *BMC Biotechnol.*, **24**, 5 (2024); https://doi.org/10.1186/s12896-023-00828-z
36. Y. Takahashi, S. Imazato, A.V. Kaneshiro, S. Ebisu, J.E. Frencken and F.R. Tay, *Dent. Mater.*, **22**, 647 (2006); https://doi.org/10.1016/j.dental.2005.08.003
37. G. Franci, A. Falanga, S. Galdiero, L. Palomba, M. Rai, G. Morelli and M. Galdiero, *Molecules*, **20**, 8856 (2015); https://doi.org/10.3390/molecules20058856
38. B.A. Makwana, D.J. Vyas, K.D. Bhatt, V.K. Jain and Y.K. Agrawal, *Spectrochim. Acta A Mol. Biomol. Spectrosc.*, **134**, 73 (2015); https://doi.org/10.1016/j.saa.2014.05.044
39. G.A. Sotiriou and S.E. Pratsinis, *Curr. Opin. Chem. Eng.*, **1**, 3 (2011); https://doi.org/10.1016/j.coche.2011.07.001
40. J. Helmlinger, C. Sengstock, C. Groß-Heitfeld, C. Mayer, T.A. Schildhauer, M. Köller and M. Epple, *RSC Adv.*, **6**, 18490 (2016); https://doi.org/10.1039/C5RA27836H
41. B. Khameneh, R. Diab, K. Ghazvini and B.S.F. Bazzaz, *Microb. Pathog.*, **95**, 32 (2016); https://doi.org/10.1016/j.micpath.2016.02.009
42. H.D. Marston, D.M. Dixon, J.M. Knisely, T.N. Palmore and A.S. Fauci, *JAMA*, **316**, 1193 (2016); https://doi.org/10.1001/jama.2016.11764
43. M. Gholami, F. Azarbani and F. Hadi, *Mater. Technol.*, **37**, 934 (2022); https://doi.org/10.1080/10667857.2021.1906390
44. F. Khan, D.T.N. Pham, S.F. Oloketuyi, P. Manivasagan, J. Oh and Y.M. Kim, *Colloids Surf. B Biointerfaces*, **185**, 110627 (2020); https://doi.org/10.1016/j.colsurfb.2019.110627
45. A. Humayun, Y. Luo, A. Elumalai and D.K. Mills, *Mater. Technol.*, **37**, 28 (2022); https://doi.org/10.1080/10667857.2020.1806188